PAPER

Protein amyloids develop an intrinsic fluorescence signature during aggregation†

Fiona T. S. Chan,[a] Gabriele S. Kaminski Schierle,[a] Janet R. Kumita,[b] Carlos W. Bertoncini,[c] Christopher M. Dobson[b] and Clemens F. Kaminski*[a]

We report observations of an intrinsic fluorescence in the visible range, which develops during the aggregation of a range of polypeptides, including the disease-related human peptides amyloid-β(1–40) and (1–42), lysozyme and tau. Characteristic fluorescence properties such as the emission lifetime and spectra were determined experimentally. This intrinsic fluorescence is independent of the presence of aromatic side-chain residues within the polypeptide structure. Rather, it appears to result from electronic levels that become available when the polypeptide chain folds into a cross-β sheet scaffold similar to what has been reported to take place in crystals. We use these findings to quantify protein aggregation *in vitro* by fluorescence imaging in a label-free manner.

Introduction

The phenomenon by which some proteins undergo structural changes from their native states into β-sheet rich fibrillar aggregates is of intense current interest, both for establishing a fundamental understanding of the process of protein misfolding and to relate the association of misfolded states with neurodegenerative diseases such as Alzheimer's disease (AD), Parkinson's disease (PD), type II diabetes and various types of amyloidosis.[1] In addition, as a biomaterial, amyloid fibrils are self-assembling supramolecular polymers with considerable stability, mechanical strength and stiffness.[2] Extensive biophysical investigations have been carried out to characterize amyloid structures in increasing detail,[3–8] but reports of spectroscopic studies that probe the electronic structure and associated photophysical properties of amyloid fibrils are scarce. Knowledge of the latter is, however, of critical importance for the development and quantitative application of fluorescent assays to probe protein self-assembly reactions. An improved understanding of amyloid photophysics is important not only for the development, application and quantification of optical assays for disease-associated amyloid formation, but also for the rational design of amyloid fibrils as novel biomaterials and nanodevices.

Recently, a fluorescence-like emission was reported for synthetic structures of peptides derived from elastin and crystalline proteins.[9–11] The structures studied were devoid of aromatic residues and extrinsic fluorescent labels, and contain a high proportion of β-sheets. The authors speculated that the phenomenon may have its origin in electron delocalisation caused by hydrogen bonds in the β-sheet structure so that low-energy electronic transitions become possible. The systems studied in the previous investigations are capable of forming β-sheet structures similar to those found in protein amyloids, and it was hypothesized therefore that amyloid fibrils may exhibit similar photophysical properties. This prompted us to investigate the photophysics of human peptides and proteins implicated in protein misfolding diseases as they aggregate to form amyloids. In this report we show conclusively that amyloid formation is concomitant with the onset of intrinsic fluorescence.

In particular, we study emergent fluorescence properties during aggregation of amyloid-β peptides and the amyloidogenic proteins tau and lysozyme,[12–14] all of which are from the human genome and associated with protein misfolding diseases.[15,16] All these polypeptides acquire intrinsic fluorescence signatures in the visible range upon aggregation. We use spectrum- and time-resolved fluorescence detection and imaging, and conclude that the observed fluorescence is a generic property of amyloid structures featuring a characteristic lifetime for each polypeptide investigated. The time-resolved fluorescence measurements exclude possible artefacts due to inelastic scattering. Intrinsic fluorescence was also detected from a fragment of amyloid-β(1–42), which is devoid of aromatics, namely amyloid-β(33–42).[17] This result shows that the phenomenon is not mediated by the presence of aromatic side chains and hence is not consistent with a previous report

[a]*Department of Chemical Engineering and Biotechnology, University of Cambridge, New Museums Site, Pembroke Street, Cambridge CB2 3RA, UK. E-mail: cfk23@cam. ac.uk; Fax: +44 (0)1223 334796*

[b]*Department of Chemistry, University of Cambridge, Lensfield Road, Cambridge CB2 1EW, UK*

[c]*Institute for Research in Biomedicine, Baldiri Reixac 10, 08028, Barcelona, Spain*

† Electronic supplementary information (ESI) available. See DOI: 10.1039/c3an36798c

that chemical modifications of aromatic residues in polypeptides during amyloid formation may lead to the formation of an intrinsic chromophore like that of GFP.[18] Rather, our results lend strong support to previous suggestions that electron delocalisation *via* hydrogen bonds in β-sheet structure can cause the phenomenon,[9–11] and they extend the validity of this argument to disease-relevant amyloid fibrils with experimental evidence. The appearance of this intrinsic fluorescence signal is concomitant with the growth of amyloid structures as detected by AFM and thus provides a direct handle for detecting amyloid formation using only optical techniques. This feature permits the study *in vitro* of amyloid self-assembly reactions without the requirement for extrinsic labelling with fluorophores, and thus eliminates any risk of perturbations due to chain modifications during aggregation.

Experimental section

Preparation of peptides and proteins

The lyophilised powder of synthetic Aβ(1–40), Aβ(1–42) and Aβ(33–42) (Bachem, Merseyside, UK), referred to as Aβ40, Aβ42, Aβ(33–42) hereafter, were prepared *via* sequential treatment with trifluoroacetic acid (TFA) and hexafluoroisopropanol (HFIP) to remove small aggregates and stored as a lyophilised film in Eppendorf tubes at −20 °C.[19] A sample was freshly thawed for each experiment. I59T human lysozyme was expressed and purified as previously described.[20] The tau construct K18 (I260C/C291A/C322A), termed K18 hereafter, was prepared as previously described.[21]

Conversion of soluble polypeptides into fibrils

Lyophilised, TFA- and HFIP-treated Aβ(1–40) and Aβ(1–42) were dissolved in 1× PBS buffer (pH 7.4) at 50 μM peptide concentration in Eppendorf tubes and incubated at 37 °C for 7 days. Lyophilised, TFA- and HFIP-treated Aβ(33–42) was initially dissolved in 1% NH₄OH at 2 mM and diluted with 1× PBS buffer (pH 7.4) to 100 μM. The sample was centrifuged (12 100 g, 10 min) to remove any undissolved peptide and the soluble fraction was incubated at 37 °C for 2 days. K18 (I260C/C291A/C322A) tau (10 μM in 50 mM ammonium acetate buffer, pH 7.0) was incubated at 37 °C for 24 h, quiescent, in the presence of 2.5 μM heparin (MW ∼ 3000, Sigma-Aldrich, Dorset, UK). I59T human lysozyme (6.8 μM in 0.1 M sodium citrate buffer, pH 5.0) was incubated at 60 °C with stirring for up to 1400 min. Hen egg white lysozyme (Sigma-Aldrich, L-6876, Lot 081K1554) was dissolved in glycine–HCl buffer, pH 2.2, filtered with 0.20 μM filters (Millipore Limited, Watford, UK), and incubated at 60 °C for up to 11 days. All buffers were made with Milli-Q water and were filtered with 0.20 μM filters (Millipore Limited, Watford, UK) before use. For the kinetic assays, aliquots were taken from the well-mixed sample at designated time points, flash frozen in liquid nitrogen and stored at −20 °C until imaged; aliquots were freshly thawed before each experiment. To dissociate the fibrils, I59T lysozyme fibrils were obtained by centrifuging at 13 400 rpm for 10 min and extracting the lower 20% of the solution.

The extract was added to 8 M guanidinium hydrochloride and left at room temperature for 24 h.

Fluorescence lifetime imaging microscopy (FLIM)

All FLIM images were recorded on a home built confocal microscopy platform based on a confocal microscope scanning unit (Olympus FluoView 300) coupled with an Olympus IX70 inverted microscope frame (Olympus UK, Essex, UK).[22,23] Acquisition of FLIM images was controlled using the software SPCM (Becker & Hickl GmbH, Berlin, Germany). For every pixel in the image (the latter consisting of 256 × 256 pixels), a histogram of photon arrival times was recorded. The image acquisition time was 500 s. It was verified that photobleaching was insignificant after image acquisition. Photon count rates were kept below 1% of the laser repetition rate to prevent photon pile-up. An instrumental response function was recorded by imaging the reflection from a cover slip. A corresponding differential interference contrast (DIC) image was also recorded for each sample for reference using the FluoView software. Images were first analysed using the software SPCImage (Becker & Hickl GmbH, Berlin, Germany). For each pixel in the image, the instrumental response function was deconvoluted from the distribution of recorded photon arrival times to produce an estimate of the fluorescence intensity decay curve that was then fitted to a mono-exponential function. Appropriate pixel binning and intensity thresholding were applied to improve the signal-to-noise ratios (SNR) and suppress background and scattering noise. The fluorescence lifetime, photon number and quality of fit (χ^2) were recorded for each pixel, producing a 256 × 256 array of values for each parameter. These data were then exported into MATLAB (Mathworks, USA) for further quantitative analysis and data presentation.

Atomic force microscopy (AFM)

AFM images were acquired using a VEECO Dimension 3100 atomic force microscope (Bruker AXS, Cambridge, UK). The instrument was operated in tapping mode in air with a silicon tip at a resonant frequency of 300 kHz, a spring constant of 40 N m⁻¹, a tip radius of 10 nm (RTESP, Bruker AXS, Cambridge, UK). Images were collected at a scan rate of 1 Hz. 5 μL of each fibrillar sample was deposited onto freshly cleaved mica surfaces for 2 h for adsorption. The samples were rinsed with 200 μL of Milli-Q water 5 times and left to dry completely in air before imaging.

Spectral measurements

Excitation and emission spectra were measured at 25 °C using a Cary Eclipse fluorescence spectrophotometer (Agilent Technologies, Oxford, UK). The excitation spectra were measured with the detection wavelength fixed at 470 nm. The emission spectra were measured with the excitation wavelength fixed at 357 nm. For all measurements, excitation and emission slit widths were 10 nm and 20 nm respectively; the PMT voltage was 750 V; the scan speed was 120 nm min⁻¹.

Confocal microscopy

A commercial confocal microscope (Leica TCS SP5, Leica Microsystems GmbH, Wetzlar, Germany) was used, with a 405 nm diode laser as the excitation source and an 63× oil immersion objective. Emission between 450 and 500 nm was recorded. Speckle noise in the fluorescence images was removed by filtering using ImageJ.

Results and discussion

Intrinsic fluorescence is a generic property of the amyloid state of proteins

During studies of a range of amyloidogenic proteins, we have observed the development of particular fluorescent features in aggregated samples. The amyloid species characterized in the present work are aggregates of the amyloid-β peptides (1–40), (1–42) and a ten-residue fragment lacking any aromatic residues (33–42),[17,24,25] the 129-residue tau protein isoform K18 (I260C/C291A/C322A variant),[12,21,26] the I59T variant of the human protein lysozyme[13,14] and hen egg white lysozyme (HEWL).[27–29] Intrinsic fluorescence measurements were performed on a custom-built confocal fluorescence microscope capable of measuring the fluorescence excitation and emission spectra, and fluorescence lifetimes with photon counting sensitivity.[22]

In Fig. 1 we show the fluorescence intensity and corresponding fluorescence emission lifetime images of the amyloid states of five peptides and proteins following excitation at 450 nm (rows 1 and 2, respectively), as well as representative fluorescence intensity decay curves (row 3) obtained by time-correlated single photon counting fluorescence lifetime imaging (TCSPC-FLIM). Analysis of the time-resolved intensity shows that the number of photons emitted in each time bin could be fitted by mono-exponential decays with lifetimes

between 2 and 4 ns (Fig. 1). By contrast, no detectable fluorescence signal was observed from solutions of the monomeric states of the peptides and proteins prior to aggregation. Aggregates were also examined using a commercial fluorescence microscope (Leica TCS SP5, Leica Microsystems GmbH, Wetzlar, Germany) with a 405 nm diode laser as the excitation source and a detection wavelength range between 450 and 500 nm. Intrinsic fluorescence could also be detected under these conditions, as shown in Fig. 2. To confirm the amyloid nature of the proteins studied here we imaged all samples also using atomic force microscopy (AFM) (Fig. 2). Furthermore, the intrinsic amyloid fluorescence could be bleached by continuous irradiation, as shown in ESI Fig. 1† for I59T lysozyme and Aβ(33–42) fibrils. When the aggregates were exposed to the denaturant guanidinium hydrochloride (at a concentration of 8 M) they dissolved completely and the sample reverted to a non-fluorescent homogeneous solution (ESI Fig. 2†), supporting further the amyloid-specific origin of the observed phenomenon.

Intrinsic amyloid fluorescence measurements permit the direct tracking of amyloid self-assembly reactions

The ability to visualize protein amyloid structures without extrinsic labelling provides opportunities for the development of in vitro kinetic aggregation assays that are not susceptible to perturbation of the aggregating protein by dyes or labels. We therefore incubated I59T lysozyme at 60 °C and pH 5.0 (conditions shown previously to generate well-defined aggregation kinetics[14]) and extracted aliquots of the reacting mixture at a series of time points during the aggregation reaction. Fig. 3 illustrates that the evolution of the intrinsic fluorescence of I59T lysozyme can be imaged by TCSPC-FLIM throughout the
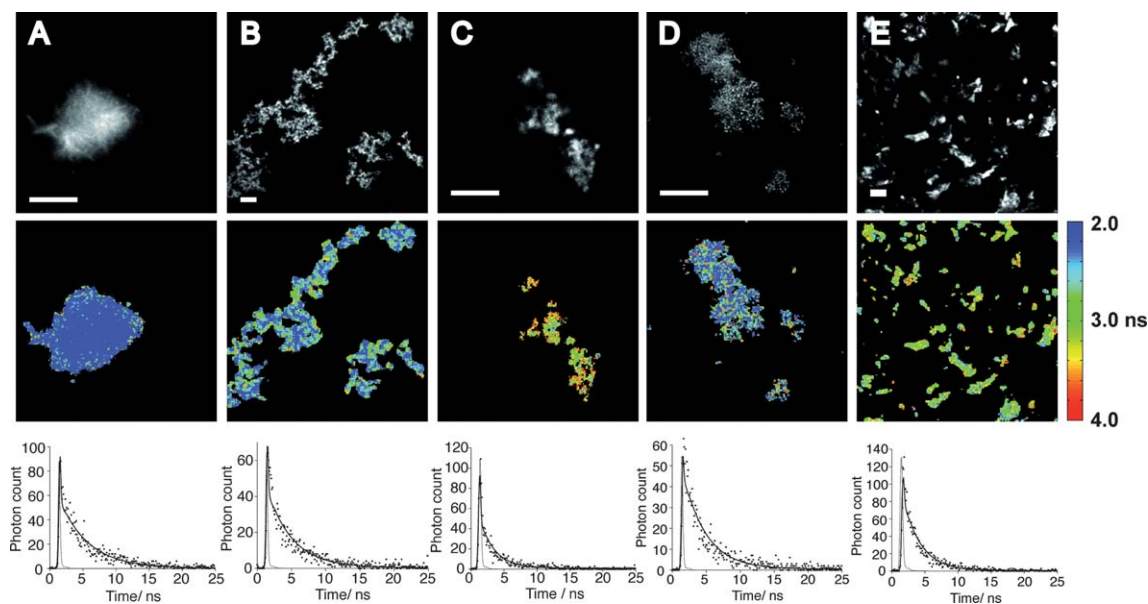

Fig. 1 Intrinsic visible fluorescence detected from five amyloid systems. Rows 1–3 represent fluorescence intensity images, fluorescence lifetime images and fluorescence intensity decay curves of the amyloid form of Aβ40 (A), Aβ42 (B), Aβ(33–42) (C), K18 tau (D) and I59T lysozyme (E). Excitation was at 450 nm wavelength and the fluorescence emission at λ > 488 nm was recorded. Scale bars, 20 μm.
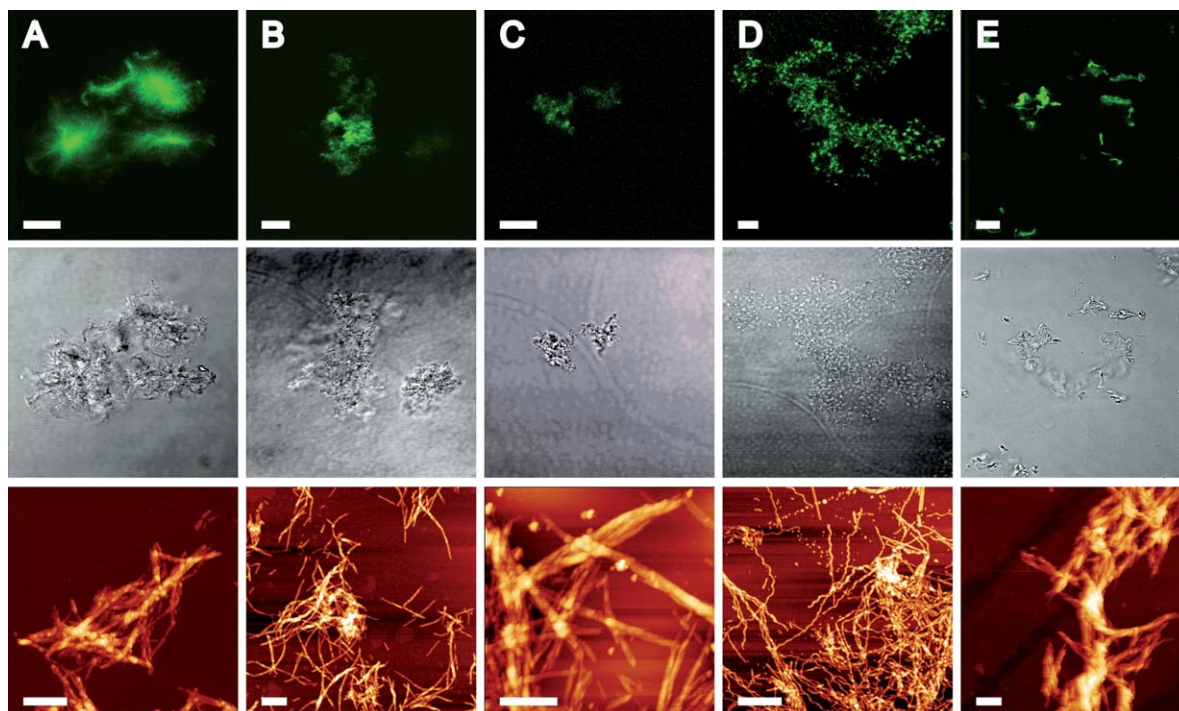
Fig. 2 Fluorescence from amyloid structures can be detected with a standard commercial imaging system. Rows 1–3 show confocal microscopy images, corresponding phase contrast images and AFM images, respectively, of Aβ40 (A), Aβ42 (B), Aβ(33–42) (C), K18 tau (D) and I59T lysozyme (E). Scale bars represent 10 μm for microscopy images, and 500 nm for AFM images.

time course of the aggregation process. Fluorescence intensity and lifetime were obtained from each aliquot and the results are shown in Fig. 3A (top and bottom rows respectively). It is clear from these images that the number of fluorescent aggregates increases with time. We further analysed the number of pixels containing a fluorescence signal in the resulting images and the fluorescence lifetimes of the aggregates. In Fig. 3B, the number of fluorescent pixels in each image is shown as a function of
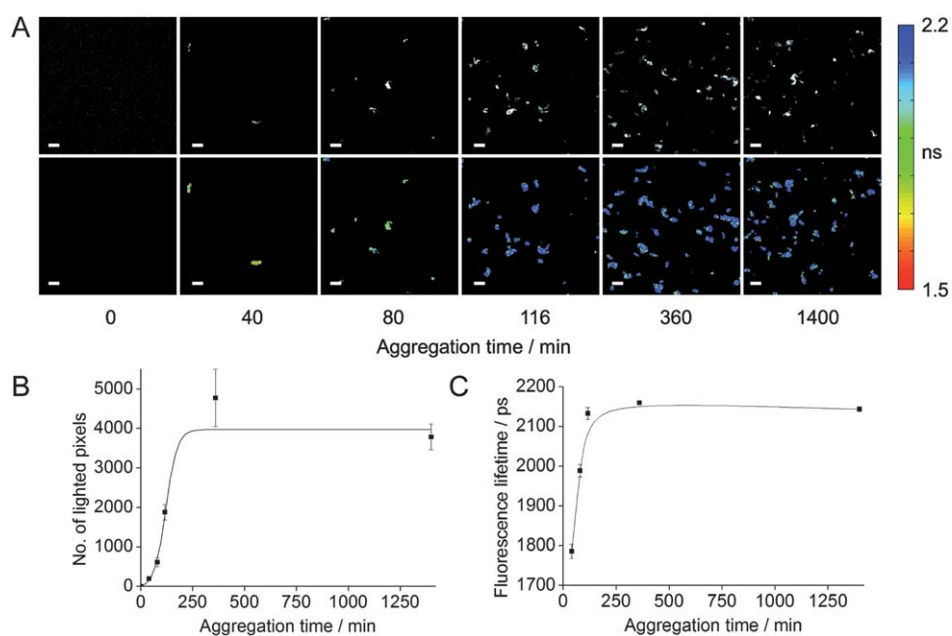

Fig. 3 The appearance of intrinsic fluorescence is closely linked to aggregation. (A) Fluorescence intensity and lifetime (rows 1 and 2 respectively) of the aggregates present at various time-points during the aggregation process (0, 40, 80, 116, 360 and 1400 min). Scale bars, 20 μm. (B) The mean number of fluorescence-containing pixels in images of the aggregates shown in (A) initially increases with aggregation time and reaches a plateau, giving a measure of the progress of fibril formation. (C) The mean emission lifetime of the fluorescence signals shown by the aggregates also increases initially with aggregation time and reaches a plateau.

aggregation time, providing a robust readout of the aggregation time course of polypeptides without any requirement for external fluorescent probes. Similarly, the lifetime of the intrinsic fluorescence from the aggregates increased monotonically with aggregation time, primarily during the fast growth phase (Fig. 3C). The evolution of intrinsic fluorescence upon amyloid formation can also be observed from time-lapse measurements of the excitation and emission spectra of hen egg white lysozyme (HEWL) during its aggregation reaction at pH 2.2 and 60 °C (ref. 27–29) using a conventional spectrofluorometer (Fig. 4A). The intensity of fluorescence emission increased with aggregation time. Spectral analysis indicated that for this protein the excitation and emission maxima are near 355 nm and 440 nm, respectively. These values are in close agreement with Guptasarma's results on concentrated solutions of recombinant bovine γ-B-crystallin and HEWL.[30] Thus, our data suggest that the fluorescence observed in soluble globular proteins is amplified upon amyloid formation when extensive β-sheets are formed, supporting Guptasarma's hypothesis that hydrogen bonding gives rise to intrinsic fluorescence in these systems. Fig. 4B shows that thioflavin T (ThT, 6 μM) binds to the HEWL fibrils formed and displays its typical excitation and emission spectra with maxima at 445 nm and 486 nm respectively, confirming the presence of amyloid structure. The intrinsic fluorescence in HEWL fibrils was dominated by the emission of ThT under these conditions.
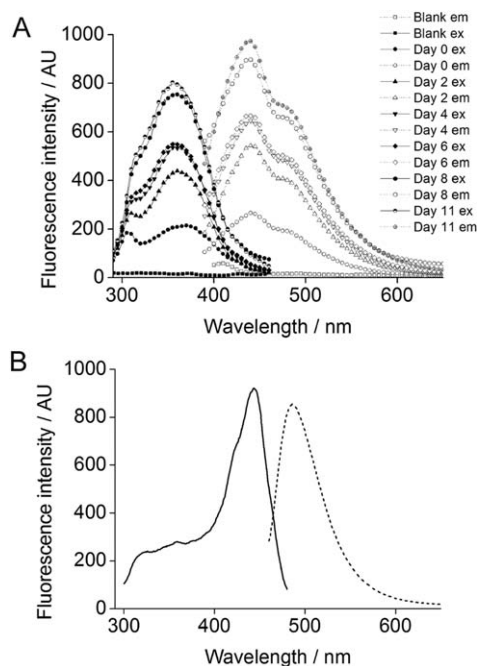
The current study provides evidence that amyloid structures, including those of relevance to human disease, can accept energy in the form of light and emit fluorescence in the visible range. Furthermore we find that the intensity of the observed fluorescence correlates with the extent of aggregation in amyloidogenic proteins. The emission signatures are Stokes-shifted from the excitation wavelength, are photobleachable and exhibit lifetimes in the nanosecond range, bearing all the hallmarks of a fluorescence process. Yet, to observe intrinsic fluorescence there is no requirement for the presence of aromatic residues in the aggregating peptide (where aromaticity often is associated with fluorescent molecules), suggesting that fluorescence originates from energy states that are specific to, and characteristic of, the molecular cross β-sheet arrangement found in all amyloid structures. The fluorescence correlates with the progress of aggregation, *i.e.* with the level of amyloid
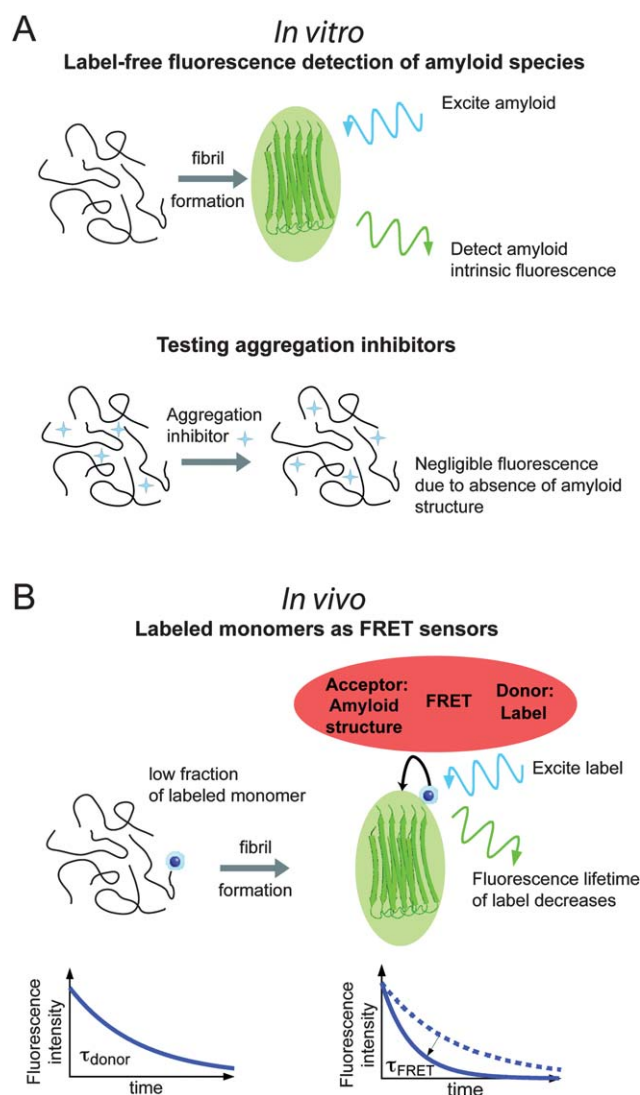

Fig. 4 Excitation and emission spectra of hen egg white lysozyme (HEWL) is closely associated with aggregation. (A) Excitation and emission spectra of hen egg white lysozyme (HEWL) at various time-points during the aggregation process (at 0, 2, 4, 6, 8, 11 days; solid line: excitation, dashed line: emission). The total fluorescence intensity increases with aggregation time. The excitation and emission maxima are at 355 nm and 440 nm respectively. (B) ThT binds to the HEWL fibrils formed and displays its typical excitation and emission maxima at 445 nm and 486 nm respectively (solid line: excitation, dashed line: emission).

Fig. 5 Strategies for sensor development using amyloid intrinsic fluorescence. (A) *In vitro* sensing of amyloid formation by detecting intrinsic fluorescence from amyloid species. (B) *In vivo* sensing of amyloid formation by detecting fluorescence lifetime changes of external fluorophores caused by FRET with amyloid structures.

structure, permitting potent readouts of the latter to be developed *in vitro* (Fig. 5), expanding the biophysical toolset available for the study of this important form of proteins[31] without the need to attach an extrinsic label as a probe of the extent of the reaction. Conventionally, fluorescent probes such as thioflavin T and Congo red have been used as reporters of aggregation because their fluorescence properties exhibit significant changes upon binding to amyloid structures. Despite their widespread application, however, the use of such probes can be prone to variability. For example, a highly aggregation-prone mutant of amyloid-β (ΔE22-Aβ(1–39), known as the Japanese mutant) had been assumed incapable of forming fibrils; in fact conclusions drawn were in error because of a reduced binding affinity of thioflavin T to the amyloid state of this peptide variant.[32] Equally, some compounds have been mistakenly identified as aggregation inhibitors because they interact directly with thioflavin T and reduce its amyloid binding capacity.[33,34] As the *in vitro* assay described here requires no chemical modification or labelling, there is no risk of any perturbation of the aggregation process. It is noted that although the intrinsic fluorescence does not require any binding of external probes, any potential inhibitors tested which are themselves fluorescent, or are fluorescence quenchers, could affect the effectiveness of this technique in certain cases.

For *in vivo* applications a readout based solely on intrinsic fluorescence is unlikely to be quantitative or reproducible because of competing autofluorescence from living cells and organisms, which reduces both the specificity and sensitivity of the assay. However, the phenomenon described here provides potential for the development of specific and sensitive *in vivo* probes *via* external fluorophores covalently attached to the amyloid backbone.[23] The latter can be specifically excited and act as donors in a hetero-FRET energy transfer processes to energy states associated with the amyloid structure (Fig. 5). The degree of FRET observed correlates with the extent of aggregation and can be readily quantified *via* concomitant donor fluorescence lifetime changes. In contrast to homoFRET,[35] only low labelling densities are required and the potential for steric perturbation of aggregation reactions is reduced.

The observation of fluorescent emission from the amyloid states of protein raises fundamental questions about the electronic structure of the amyloid state of polypeptide molecules. In Fig. 3C we show that the lifetime of the intrinsic fluorescence from the aggregate of species increases monotonically with aggregation time, notably during the fast growth phase, which suggests that the phenomenon is intrinsically linked to the molecular structural changes taking place during amyloid formation. Thus, the lifetime of the intrinsic fluorescence provides extra information on the formation of amyloid structures, in addition to the quantity of insoluble aggregates as shown in Fig. 3A and B. Similar accounts of strong UV-A fluorescence emission from β-sheet rich structures have suggested that the formation of extensive arrays of hydrogen bonds may give rise to sufficient delocalisation of the electrons associated with the formation of hydrogen bonds, which could then give rise to optically excitable energy states[9–11] (illustrated in ESI

Fig. 3†). A detailed understanding of the electronic transitions that could give rise to the observed optical properties is, however, still required. Quantum mechanical studies on model amyloid systems have been reported, which show that hydrogen bonds in the amyloid state are cooperative and contribute to the stability of the cross-β structures.[36,37] We envisage that the experimental evidence reported in the present study will encourage studies in the future of the excited electronic states of amyloid systems. Further spectroscopic studies on a wide range of different amyloid systems should, therefore, yield new molecular-level structural information as well as enable the process of amyloid formation to be monitored with fluorescence techniques in a label-free manner.

References

1 F. Chiti and C. M. Dobson, *Annu. Rev. Biochem.*, 2006, **75**, 333–366.

2 J. F. Smith, T. P. J. Knowles, C. M. Dobson, C. E. Macphee and M. E. Welland, *Proc. Natl. Acad. Sci. U. S. A.*, 2006, **103**, 15806–15811.

3 A. T. Petkova, Y. Ishii, J. J. Balbach, O. N. Antzutkin, R. D. Leapman, F. Delaglio and R. Tycko, *Proc. Natl. Acad. Sci. U. S. A.*, 2002, **99**, 16742–16747.

4 C. P. Jaroniec, C. E. MacPhee, V. S. Bajaj, M. T. McMahon, C. M. Dobson and R. G. Griffin, *Proc. Natl. Acad. Sci. U. S. A.*, 2004, **101**, 711–716.

5 T. Lührs, C. Ritter, M. Adrian, D. Riek-Loher, B. Bohrmann, H. Döbeli, D. Schubert and R. Riek, *Proc. Natl. Acad. Sci. U. S. A.*, 2005, **102**, 17342–17347.

6 R. Nelson, M. R. Sawaya, M. Balbirnie, A. Ø. Madsen, C. Riekel, R. Grothe and D. Eisenberg, *Nature*, 2005, **435**, 773–778.

7 G. S. Kaminski Schierle, S. van de Linde, M. Erdelyi, E. K. Esbjörner, T. Klein, E. Rees, C. W. Bertoncini, C. M. Dobson, M. Sauer and C. F. Kaminski, *J. Am. Chem. Soc.*, 2011, **133**, 12902–12905.

8 M. Ahn, E. De Genst, G. S. Kaminski Schierle, M. Erdelyi, C. F. Kaminski, C. M. Dobson and J. R. Kumita, *PLoS One*, 2012, **7**, e50192.

9 A. Shukla, S. Mukherjee, S. Sharma, V. Agrawal, K. V. Radha Kishan and P. Guptasarma, *Arch. Biochem. Biophys.*, 2004, **428**, 144–153.

10 L. L. del Mercato, P. P. Pompa, G. Maruccio, A. Della Torre, S. Sabella, A. M. Tamburro, R. Cingolani and R. Rinaldi, *Proc. Natl. Acad. Sci. U. S. A.*, 2007, **104**, 18019–18024.

11 S. Sharpe, K. Simonetti, J. Yau and P. Walsh, *Biomacromolecules*, 2011, **12**, 1546–1555.

12 E. Mandelkow, M. Von Bergen, J. Biernat and E.-M. Mandelkow, *Brain Pathol.*, 2007, **17**, 83–90.

13 J. R. Kumita, S. Poon, G. L. Caddy, C. L. Hagan, M. Dumoulin, J. J. Yerbury, E. M. Stewart, C. V. Robinson, M. R. Wilson and C. M. Dobson, *J. Mol. Biol.*, 2007, **369**, 157–167.

14 C. L. Hagan, R. J. K. Johnson, A. Dhulesia, M. Dumoulin, J. Dumont, E. De Genst, J. Christodoulou, C. V. Robinson, C. M. Dobson and J. R. Kumita, *Protein Eng. Des. Sel.*, 2010, **23**, 499–506.

15 L. Mucke and D. J. Selkoe, *Cold Spring Harbor Perspect. Med.*, 2012, **2**, a006338.

16 A. de Calignon, M. Polydoro, M. Suárez-Calvet, C. William, D. H. Adamowicz, K. J. Kopeikina, R. Pitstick, N. Sahara, K. H. Ashe, G. A. Carlson, T. L. Spires-Jones and B. T. Hyman, *Neuron*, 2012, **73**, 685–697.

17 H. Li, B. H. Monien, E. A. Fradinger, B. Urbanc and G. Bitan, *Biochemistry*, 2010, **49**, 1259–1267.

18 O. Tcherkasskaya, *Protein Sci.*, 2007, **16**, 561–571.

19 A.-C. Brorsson, B. Bolognesi, G. G. Tartaglia, S. L. Shammas, G. Favrin, I. Watson, D. A. Lomas, F. Chiti, M. Vendruscolo, C. M. Dobson, D. C. Crowther and L. M. Luheshi, *Biophys. J.*, 2010, **98**, 1677–1684.

20 J. R. Kumita, R. J. K. Johnson, M. J. C. Alcocer, M. Dumoulin, F. Holmqvist, M. G. McCammon, C. V. Robinson, D. B. Archer and C. M. Dobson, *FEBS J.*, 2006, **273**, 711–720.

21 S. Barghorn and E. Mandelkow, *Biochemistry*, 2002, **41**, 14885–14896.

22 J. H. Frank, A. D. Elder, J. Swartling, A. R. Venkitaraman, A. D. Jeyasekharan and C. F. Kaminski, *J. Microsc.*, 2007, **227**, 203–215.

23 G. S. Kaminski Schierle, C. W. Bertoncini, F. T. S. Chan, A. T. van der Goot, S. Schwedler, J. Skepper, S. Schlachter, T. van Ham, A. Esposito, J. R. Kumita, E. A. A. Nollen, C. M. Dobson and C. F. Kaminski, *ChemPhysChem*, 2011, **12**, 673–680.

24 T. Iwatsubo, A. Odaka, N. Suzuki and H. Mizusawa, *Cell*, 1994, **13**, 45–53.

25 E. McGowan, F. Pickford, J. Kim, L. Onstead, J. Eriksen, C. Yu, L. Skipper, M. P. Murphy, J. Beard, P. Das, K. Jansen, M. DeLucia, W.-L. Lin, G. Dolios, R. Wang, C. B. Eckman, D. W. Dickson, M. Hutton, J. Hardy and T. Golde, *Neuron*, 2005, **47**, 191–199.

26 S. Barghorn, Q. Zheng-Fischhöfer, M. Ackmann, J. Biernat, M. von Bergen, E.-M. Mandelkow and E. Mandelkow, *Biochemistry*, 2000, **39**, 11714–11721.

27 M. R. H. Krebs, D. K. Wilkins, E. W. Chung, M. C. Pitkeathly, A. K. Chamberlain, J. Zurdo, C. V. Robinson and C. M. Dobson, *J. Mol. Biol.*, 2000, **300**, 541–549.

28 E. Frare, P. Polverino de Laureto, J. Zurdo, C. M. Dobson and A. Fontana, *J. Mol. Biol.*, 2004, **340**, 1153–1165.

29 L. N. Arnaudov and R. de Vries, *Biophys. J.*, 2005, **88**, 515–526.

30 P. Guptasarma, *Arch. Biochem. Biophys.*, 2008, **478**, 127–129.

31 C. W. Bertoncini and M. S. Celej, *Curr. Protein Pept. Sci.*, 2011, **12**, 205–220.

32 A. L. Cloe, J. P. R. O. Orgel, J. R. Sachleben, R. Tycko and S. C. Meredith, *Biochemistry*, 2011, **50**, 2026–2039.

33 K. Zovo, E. Helk, A. Karafin, V. Tõugu and P. Palumaa, *Anal. Chem.*, 2010, **82**, 8558–8565.

34 A. Noormägi, K. Primar, V. Tõugu and P. Palumaa, *J. Pept. Sci.*, 2012, **18**, 59–64.

35 F. T. S. Chan, C. F. Kaminski and G. S. Kaminski Schierle, *ChemPhysChem*, 2011, **12**, 500–509.

36 K. Tsemekhman, L. Goldschmidt, D. Eisenberg and D. Baker, *Protein Sci.*, 2007, **16**, 761–764.

37 O. Přenosil, M. Pitoňák, R. Sedlák, M. Kabeláč and P. Hobza, *Z. Phys. Chem.*, 2011, **225**, 553–574.